Check for updates

Accepted Article

A dendritic polymer-based nanosystem mediates drug penetration and irreversible endoplasmic reticulum stresses in tumor via neighboring effect

*Xiuli Zheng, Dayi Pan, Guonian Zhu, Lu Zhang, Apanpreet Bhamra, Rongjun Chen, Hu Zhang, Qiyong Gong, Zhongwei Gu, Kui Luo**

Dr. X. L. Zheng, Dr. D. Y. Pan, G.N. Zhu, Prof. Q. Y. Gong, Prof. Z. W. Gu, Prof. K. Luo

Huaxi MR Research Center (HMRRC), Department of Radiology, National Clinical Research Center for Geriatrics, Frontiers Science Center for Disease-Related Molecular Network, State Key Laboratory of Biotherapy, West China Hospital, Sichuan University, Chengdu, 610041, China

*E-mail: luokui@scu.edu.cn (Prof. Luo)

G.N. Zhu, L. Zhang

Laboratory of Clinical Proteomics and Metabolomics, Institutes for Systems Genetics, and Core Facility of West China Hospital, West China Hospital, Sichuan University, Chengdu, 610041, China

A. Bhamra, Dr. R. Chen

Department of Chemical Engineering, Imperial College London, South Kensington Campus, London, SW7 2AZ, United Kingdom

Prof. H. Zhang

Amgen Bioprocessing Centre, Keck Graduate Institute, Claremont, CA 91711, USA

Prof. Q. Y. Gong, Prof. K. Luo

Functional and molecular imaging Key Laboratory of Sichuan Province, and Research Unit of Psychoradiology, Chinese Academy of Medical Sciences, Chengdu, 610041, China

Keywords: neighboring effect, drug penetration, endoplasmic reticulum stresses, combination therapy, drug delivery

This article has been accepted for publication and undergone full peer review but has not been through the copyediting, typesetting, pagination and proofreading process, which may lead to differences between this version and the Version of Record. Please cite this article as doi: 10.1002/adma.202201200.

This article is protected by copyright. All rights reserved.

Accepted Article

Nanoparticles (NPs)-based cancer therapeutics is generally impeded by poor drug penetration into solid tumors due to their dense tumor extracellular matrix (ECM). Herein, we develop pH/redox-responsive dendritic polymer-based NPs to amplify the neighboring effect for improving drug penetration and driving cell apoptosis via combination therapy. Pyropheophorbide a (Ppa) is conjugated with PEGylated dendritic peptides via disulfide bonds and doxorubicin (DOX) encapsulated in the conjugate to construct dual-responsive NPs, PDPP@D. Delayed released DOX and Ppa from PDPP@D exert their combination therapeutic effect to induce cell apoptosis, and then they are liberated out of dying cells to amplify the neighboring effect, resulting in their diffusion through the dense ECM and penetration into solid tumors. Transcriptome studies reveal that PDPP@D leads to irreversible stress on the endoplasmic reticulum and inhibits cell protection through blocking the IRE1-dependent survival pathway and unleashing the DR5-mediated caspase activity to promote cell death. The strategy of amplifying the neighboring effect of NPs through combination therapy may offer great potential in enhancing drug penetration and eradicating solid tumors.

1. Introduction

Nanoparticles (NPs) that have a shrinkable size and/or a switchable charge can be tuned for structural deformation in the tumor microenvironment can remarkably improve pharmacokinetics of encapsulated drugs and enhance their penetration in solid tumors, therefore, these NPs have the great potential for next generation drug delivery and tumor therapy.[1] Although size, charge and shape changes of these NPs could improve transportation of NPs in tumor tissues, physical and chemical properties of the tumor microenvironment may significantly impede the penetration of NPs at a therapeutic concentration.[2] A dense extracellular matrix (ECM), a high cell packing density, an elevated interstitial flow pressure and a slow interstitial flow velocity constitute a variety of tumor microenvironment barriers.[3] NPs that reach the tumor sites are dominantly hijacked by stroma cells, and their penetration in the tumor mass is greatly retarded by a dense network of the ECM.[4] Nano-carriers, such as liposomes, viruses, and polymers, have a size of tens to hundreds of nanometers, and they often need to overcome the barrier of the interlaced network of the ECM so that they can achieve deep penetration in the tumor tissue.[5]

The neighboring effect was found to improve the penetration of drug-loaded NPs and boost cytotoxicity of the drug in tumor masses.[6] Because of the neighboring effect, tumor cells may become in-situ drug depots after their uptake of drug-loaded NPs, and the drug could be released

This article is protected by copyright. All rights reserved.

Accepted Article

from dying cells produced by drug induced apoptosis to kill surrounding cells. Through the intracellular-to-intercellular delivery cycle, the drug could gradually move to the interior of tumors. Notably, the NPs with the neighboring effect have a greater ability to retain high retention in tumor tissues due to a mechanism known as enhanced permeability and retention (EPR) effect.[7] In addition, free drugs readily penetrate through the ECM by faster convective transport in comparison with much slower diffusion of NPs.[8] Compared with burst release of a drug from NPs, delayed release of the drug could prolong its period of action, allowing more drug to be released to kill neighboring tumor cells, thus achieving the greatest enhancement in intercellular penetration in the tumor tissue.[6] Therefore, NPs with strong tumor retention and delayed drug release could amplify the neighboring effect to achieve uniform drug distribution throughout the entire tumor tissues and elevated antitumor effects.

Supramolecular peptide is a novel self-delivery nano-platform for drug conjugates that offers a range of advantages, such as facile fabrication, high drug-loading capacity, prolonged blood circulation, and decreased carrier-related toxicity.[9] Recently, we have reported that a PEGylated dendritic peptide-pyropheophorbide a (Ppa) conjugate, PDPP, can assemble into self-stabilized nanoparticles with enhanced tumor retention and stable delivery of Ppa for highly-efficient photodynamic therapeutic effects.[10] This study demonstrates the self-stabilized nanoparticles based on PEGylated dendritic peptides are promising for tumor therapy. However, challenges remain to improve the antitumor efficacy because Ppa cannot be released from PDPP to achieve the neighboring effect for deep tumor penetration. In addition, stimuli-responsive NPs have been widely studied due to a differential pH/redox/ATP level in the tumor microenvironment.[11] As a result, self-assembled NPs with pH/redox-responsive drug liberation offer great potential for application in tumor penetration.

Accordingly, we developed pH- and redox-responsive NPs, PDPP@D, to augment penetration and efficacies of Ppa and DOX at the tumor site via the neighboring effect (**Figure 1**). After intravenous administration, PDPP@D that had a negative charge in the PEG shell during blood circulation could efficiently accumulate at the tumor site, and it could be subsequently internalized by the cells at the outer layer of the tumor tissue. A low endosomal/lysosomal pH could promptly protonate the amino group of DOX and a high level of cytosolic glutathione (GSH) could efficiently trigger the cleavage of

This article is protected by copyright. All rights reserved.

Accepted Article

the disulfide bond to release DOX and Ppa from PDPP@D, respectively. The released DOX and Ppa could induce apoptosis of tumor cells by combination therapy. Both drugs that were liberated from dead cells could be transferred into neighboring cancer cells, ultimately reaching the center of the solid tumor. Administration of PDPP@D was found to up-regulate PKR-like ER kinase (PERK) to activate the endoplasmic reticulum (ER) stress. PDPP@D treatment with laser irradiation could strengthen this stress to raise the mRNA level of death receptor 5 (DR5) to mediate increased activity of caspase and drive the apoptosis. Notably, inositol requiring 1 (IRE1)-associated cell protection was significantly impaired. Therefore, the synthesized PDPP@D could facilitate effective delivery of two antitumor drugs to the deep tumor tissue via the neighboring effect, leading to irreversible ER stresses and impaired cell protection for destroying the entire solid tumor. This study offers a potential nano-platform to enhance drug penetration into deep tumor tissues for efficacious antitumor therapy.

2. Results

2.1. Synthesis and characterization of PDPP@D

In this study, NPs were designed by harnessing the neighboring effect to enhance drug penetration in tumors. To achieve this objective, NPs should possess strong tumor retention, and drugs should preferably be released in the delayed manner. Meanwhile, apoptosis of tumor cells could be significantly induced via combination therapy, ultimately resulting in a strong neighboring effect. In our previous report, we developed an amphiphilic conjugate, PDPP, which was capable to be utilized as a nano-carrier to deliver payloads (drugs, genes or dyes) with ultrahigh stability and high tumor retention for photodynamic therapy of tumors[10]. Herein, we exploited the ultrahigh stable nature of PDPP to design dual-responsive NPs (PDPP@D), which could not only achieve delayed release of DOX/Ppa for combination therapy,[12] but also amplify the neighboring effect to eliminate the entire tumor tissue.

As one of the computational simulation methods, dissipative particle dynamics (DPD) simulation is appropriate for complex drug delivery systems, and employed to investigate the self-assembly process of PDPP@D (Scheme S1 and Table S1, Supporting Information).[13] First, we investigated the loading capacity of PDPP for DOX, as well as the self-assembly structure of PDPP@D. DPD

This article is protected by copyright. All rights reserved.

Accepted Article

simulations on the DOX-loaded PDPP@D at different ratios of DOX to PDPP ranging from 1/5 to 30/1 were conducted and the results were shown in **Figure 2A** and Figure S1 (Supporting Information). PDPP and DOX were initially randomly dispersed in the simulation box to form a homogeneous solution. With increasing time, PDPP gradually aggregated to form small core-shell clusters and DOX was captured inside the core of PDPP after 12000 simulation steps. Subsequently, small clusters interacted with each other to form larger aggregates after 60000 steps, and finally a large single spherical micelle was formed after 1,000,000 steps. At 3,000,000 simulation steps, free DOX was observed to diffuse into the spherical micelle. When the simulation step increased, no observable change in the shape and size of the spherical micelle was found, indicating that microphase separation of this system reached dynamic equilibrium and a stable DOX-loaded micelle was eventually formed. In this equilibrium state, DOX was physically encapsulated in the assembly core, while PDPP was located in the shell region. It was worth noting that increasing DOX content did gradually influence the micelle structure. As the ratio of DOX to PDPP increased from 1/5 to 5/1, the majority of DOX could be encapsulated inside the micelle, however, when the ratio of DOX to PDPP increased from 15/1 to 30/1, the micelle could not encapsulate all of DOX, leading to a reduced entrapment efficiency of DOX and an increased exposure level of DOX outside the surface of the micelle (Figure S2A, Supporting Information). The density distributions of DOX at the ratio of DOX to PDPP from 1/5 to 5/1 were clearly shown in Figure S2B (Supporting Information) as radial distribution function curves. These simulation results suggested that with an increase in the DOX content, DOX was initially confined inside the micelle core, then gradually migrated to the interface between the hydrophobic core and the hydrophilic PEG shell, and finally exposed to the surface of the micelle. By carefully manipulating the ratio of DOX to PDPP, PDPP could form stable micelles in an aqueous solution and DOX could be well encapsulated inside the micelles. Therefore, the feed ratio of DOX to PDPP was suggested to be 1/5~5/1 to prepare PDPP@D.

Then, PDPP was prepared in accordance with previously reported studies (Scheme S2 and Figure S3-7, Supporting Information)[10]. Subsequently, both PDPP and DOX were dissolved thoroughly in dimethyl sulfoxide (DMSO) at the feed ratio recommended from DPD simulations, and the mixture was dropwise added into an aqueous medium under ultrasonic conditions. Supramolecular interactions drove the formation of self-assembly nanoparticles and synchronous encapsulation of

This article is protected by copyright. All rights reserved.

Accepted Article

DOX. As shown in differential scanning calorimetry (DSC) curves in Figure 2B, an endothermic peak of DOX appeared at about 231.63 □ for DOX·HCl and 237.60 □ for the physical mixture of DOX·HCl and PDPP. However, this endothermic peak of DOX·HCl disappeared in the curve of PDPP@D, implying that DOX was wrapped in the nanoparticles in amorphism. The loading content of Ppa and DOX was about 14.3% and 6.9%, respectively, determined via a UV-Vis spectrophotometer (Figure S8, Supporting Information). In the aqueous solution, PDPP was able to self-assemble into nanostructures, and the critical assembly concentration (CAC) of PDPP was determined to be 2.44 μg mL^{-1} (Figure S9, Supporting Information). The photophysical properties of PDPP and PDPP@D revealed that fluorescence of Ppa and DOX was quenched in the assembled nanoparticles, but their fluorescence was successfully recovered when the assembled structure was disrupted with a surfactant, sodium dodecyl sulfate (SDS) (Figure S10, Supporting Information). Similar observations were observed in the UV-vis absorption spectra of PDPP and PDPP@D (Figure S11, Supporting Information), indicating that the hydrophobic force and π–π stacking of Ppa and DOX could intensify the aggregation-induced quenching effect in PDPP and PDPP@D. In addition, both PDPP and PDPP@D possessed better resistance against photo-bleaching in comparison with Ppa because of their stable and intact self-assembled nanostructures as their absorbance remained after laser irradiation in an intact (in H_2O) or a disrupted (in DMSO) structure (Figure S12, Supporting Information). To determine the feasibility of using PDPP@D for photodynamic therapy (PDT), the molar extinction coefficient, fluorescence quantum yield and singlet oxygen quantum yield of PDPP and PDPP@D were examined and compared with Ppa. As shown in Figure S13 and Table S2 (Supporting Information), the above three parameters of PDPP and PDPP@D were slightly lower than those of Ppa, indicating both PDPP and PDPP@D may be used as a photosensitizer for PDT. Moreover, there were no significant differences in the above three parameters between PDPP and PDPP@D. These data demonstrated that neither the self-assembly nor the DOX encapsulation in PDPP affected the photo-properties of Ppa in PDPP@D.

In our previous study, we have identified that a hydrophile-lipophile balance (HLB) value has a significant impact on the physicochemical features of amphiphiles, and the HLB value may directly affect the size of amphiphiles with self-assembled nanostructures.[14] In this study, Ppa was a hydrophobic chlorophyll-derived porphyrin analogue that had similar chemical properties and

This article is protected by copyright. All rights reserved.

Accepted Article

structures (e.g., hydrophobic, aliphatic and aromatic) as hydrophobic DOX. Therefore, wrapping DOX into one nanoparticle would reduce its HLB value, ultimately affecting the morphology and size of the nanoparticle. Furthermore, non-covalent interactions between Ppa and DOX would impact the self-assembly behavior of the nanoparticle. As shown from dynamic light scattering (DLS) measurements (Figure 2C and Table S3, Supporting Information), both PDPP and PDPP@D exhibited a weak negative charge, but PDPP@D (56 nm) was smaller than PDPP (about 150 nm), which was consistent with transmission electron microscopy (TEM) observations (Figure 2D). Moreover, non-covalent interactions on self-assembly of PDPP and PDPP@D, such as hydrophobic effect, hydrogen bonding or ionic interaction, were investigated. As observed in Figure 2E and Figure S14 (Supporting Information), both PDPP and PDPP@D had no significant change in the hydrodynamic diameter after dispersion in the NaCl or urea solutions at all tested concentrations, but disassembly of both of them occurred in the Triton X-100 solution at high concentrations due to hydrophobic competition, which supported that the hydrophobic force may be the most important driving force for self-assembly of PDPP and PDPP@D. The hydrodynamic diameter and PDI of PDPP and PDPP@D in PBS with 10% FBS remained unchanged for 72 h (Figure 2F-G and Figure S15, Supporting Information), indicating both nanoparticles could maintain a stable self-assembled structure in a physiological condition. These results suggested that both PDPP and PDPP@D could have long-term colloidal stability and possess resistance to protein adsorption, leading to a prolonged blood circulation with enhanced tumor retention for NPs.

To examine the sensitivity of dual-responsive PDPP@D to biological stimuli such as an acidic pH and an elevated intracellular redox milieu proposed in Figure 1, a microplate spectrophotometer, DLS and TEM were used to reveal the release kinetics of PDPP@D under different conditions (Figure 2H). PDPP@D could maintain its structural stability with ~20% of DOX released after 12 h incubation at a physiological pH. It was interesting to note that DOX release from PDPP@D increased to 32% at pH 7.4 in the presence of 10 mM GSH, due to cleavage of the disulfide bond in PDPP@D. Only 60% of DOX was released in 60 h under the same release condition, as release of DOX from PDPP@D was strongly inhibited by hydrophobic interaction between DOX and PDPP. However, the release of DOX was substantially increased and 71% of DOX was released from PDPP@D in 60 h at pH 5.2 owing to pH-induced protonation. Additionally, 78% of DOX released from PDPP@D release in 60 h was

This article is protected by copyright. All rights reserved.

Accepted Article

observed at pH 5.2 in the presence of 10 mM GSH. The delayed release of Ppa was also confirmed in the presence of GSH (Figure S16, Supporting Information). Additionally, the delayed release of DOX was in accordance with size changes of PDPP@D under these release conditions (Figure 2I and Figure S17, Supporting Information). PDPP@D maintained an average size of about 60 nm with a PEG outer shell at pH 7.4, which was beneficial for transportation of the micelle in the blood and retention in the tumor tissue due to the EPR effect. However, PDPP@D expanded to 560 nm due to cleavage of the disulfide bond in PDPP@D in the presence of 10 mM GSH at 12 h, while it could retain a stable nanostructure due to the PEG outer shell. From 12 h to 24 h, cleavage of the disulfide linkage between hydrophilic PDP and hydrophobic Ppa led to disassociation of PDPP@D into bigger loose aggregates. Similar observations were applied to the size evolution of PDPP@D in pH 5.2 with 10 mM GSH. TEM images of PDPP@D in Figure 2J also supported that the size distribution of particles shifted from a nano-meter scale to a micron meter scale at 24 h (pH 5.2 with 10 mM GSH). With a decrease in pH and in the presence of GSH, Ppa and DOX was released from PDPP@D to result in a disturbance in the HLB value of PDPP@D. Thus, the nanostructure experienced structural changes from a fully packed structure in the form of nanoparticles to a loosely packed structure in the form of microparticles and then irregularly micro-sized aggregates. Ultimately, the disulfide bonds of these aggregates were cleaved by GSH and small degraded fragments were formed (Figure 2K). Delayed release of DOX played important roles in structural transformation of PDPP@D, which may prolong the action period of the drug and allow it to repeatedly infect more tumor cells to obtain the optimum penetration by boosting neighboring effect.

2.2. The neighboring effect of PDPP@D

To confirm PDPP@D had the neighboring effect to release drugs from apoptotic cells and then induce cell death of the surrounding cells, fresh cells were treated with the spent medium from PDPP@D-treated cells. As shown in **Figure 3A**, 4T1 cells were first incubated with PDPP@D for 2, 8, or 24 h and subsequently irradiated by a laser. The liberated NPs and free drugs in the medium from dying cells were separated and collected. The spent medium from non-irradiated cells were also collected as a control. The collected medium at different time points was transferred and incubated with fresh cells with or without laser irradiation.

This article is protected by copyright. All rights reserved.

Accepted Article

The released products in the spent medium from 4T1 cells treated with PDPP@D for 2, 8, and 24 h with or without laser irradiation were analyzed by LC/MS. Compared with the retention time in the LC/MS spectra for standard samples (free DOX and Ppa), the released products from dying cells had a consistent retention time of 2.5 min for DOX and 5.7 min for Ppa under the same analytical condition (Figure 3B and Figure S18-31, Supporting Information). To further characterize these chemical compositions, the mass spectrometry (MS, MS1) of their parent ions and tandem mass spectrometry (MS/MS, MS2) of their daughter ions were compared with those for standard samples (free DOX and Ppa) under the same analytical condition. The molecular ion peaks at m/z 544.18 in the MS spectrum of the released products from dying cells were assigned to $[M+H]^+$ of DOX and m/z 535.27 to $[M+H]^+$ of Ppa, which were in agreement with those of standard samples (Figure 3C and Figure S18-31, Supporting Information). The diagnostic ions in the MS2 spectrum (daughter ions) also displayed consistent peaks at m/z 397.09 for DOX and m/z 535.27 for Ppa in comparison with free DOX and Ppa (Figure 3C and Figure S18-31, Supporting Information). These results indicated that the intracellular drugs from dying cells treated by PDPP@D could be released to the cell culture medium. Quantitative analyses of released DOX and Ppa from treated cells in the medium were also performed according to the MS1 and MS2 spectra. The concentrations of DOX and Ppa in the spent medium were calculated using standard curves fitted by the weighted least-square method. As shown in Figure 3D-E, the spent medium from irradiated cells had a significantly higher concentration of DOX and Ppa than that from un-irradiated cells, which demonstrated that PDPP@D with laser irradiation could improve the release of drugs from treated cells. In addition, the spent medium with a longer incubation time induced higher cytotoxicity for the fresh cells as shown in Figure 3F. Furthermore, the spent medium from irradiated cells was more toxic than that from non-irradiated cells (Figure 3F). This result indicated the combination therapy of PDPP@D could enhance the neighboring effect, which led to enhanced uptake of drugs by surrounding cells and better cytotoxicity to neighboring cells.

2.3. PDPP@D Enhanced drug penetration via the neighboring effect

Once successful fabrication of dual-responsive PDPP@D was confirmed, we first evaluated its tumor penetration mediated by the neighboring effect *in vitro*. After 3 h of incubation, cells cultured with PDPP and PDPP@D displayed strong fluorescent intensity in the cytoplasm, and DOX was

This article is protected by copyright. All rights reserved.

Accepted Article

completely packaged in PDPP@D evidenced with overlapping of red and green fluorescence (Figure S32, Supporting Information). A time-dependent increase in the fluorescence intensity was revealed by the flow cytometry due to a gradual increase in cellular uptake of Ppa, DOX, PDPP and PDPP@D from 2 h to 24 h, and the cellular uptake efficiency of both Ppa and DOX was higher than that of PDPP and PDPP@D, which may be ascribed to a smaller molecule structure of both Ppa and DOX with a rapid entry rate into cells (Figure S33, Supporting Information). Remarkably, PDPP@D was internalized by 4T1 cells more efficiently compared to PDPP, due to a smaller size of PDPP@D than PDPP. To further confirm size-dependent internalization, we examined cellular internalization pathways and subsequent intracellular trafficking of PDPP@D in 4T1 cells (Figure S34, Supporting Information). Flow cytometry results indicated that the cellular uptake of both PDPP@D and PDPP were completely blocked at 4 °C, which suggested the internalization of both of them could be an energy-dependent process.[15] It was also founded that a significantly lower amount of PDPP@D was internalized at 4 °C compared to PDPP. These results implied that internalization of PDPP@D would demand a higher level of energy consumption in tumor cells due to its significantly smaller size.

Multicellular spheroids (MTS) were then employed as an *in vitro* three-dimensional (3D) model mimicking the 4T1 tumor tissue to evaluate penetration of Ppa, DOX, PDPP and PDPP@D (Figure S35-36, Supporting Information).[16] After incubation of MTS with four components for 3 h, DOX (green) was clearly seen inside the MTS although the intensity was low, whereas Ppa (red) was only shown on the outer layer of the MTS, which may be due to poor distribution of Ppa. Excitingly, stronger Ppa fluorescence signal was observed in the periphery of the MTS after incubation with PDPP and PDPP@D, and DOX (green) of PDPP@D was evenly distributed within the spheroids, indicating Ppa penetration was enhanced in the periphery of the MTS and DOX penetration throughout the MTS, which were in alignment with the cellular uptake results and the hypothesis in Figure 1. This 3D model was also employed to investigate whether PDPP@D amplified the neighboring effect to enhance its tumor penetration. Because cell apoptosis is essential for the neighboring effect to liberate the remaining NPs for the surrounding cells, laser irradiation was imposed to achieve higher cytotoxicity. Compared to PDPP@D without laser, PDPP@D treatment with laser irradiation resulted in remarkably stronger fluorescence signal of both Ppa and DOX distributed throughout the MTS, particularly for the signal in the interior of the MTS (**Figure 4A**-C).

This article is protected by copyright. All rights reserved.

Accepted Article

Owing to the combination therapeutic effect of PDPP@D, the amplified neighboring effect resulted in more effective penetration into MTS of both drugs.

Blood clearance kinetics studies indicated that both PDPP and PDPP@D possessed a longer circulation time in comparison with Ppa, and *in vivo* stability of Ppa was enhanced after its coupling with PEGylated dendritic peptides. Both PDPP and PDPP@D as stable nanoparticles had significant impact on blood clearance kinetics that largely increased the half-life of Ppa, and PDPP@D resulted in highest prolonged half-life of ~22.9 h (Figure 4D and Table S4, Supporting Information). In addition, PDPP@D did not leak DOX in the mouse plasma and significantly prolonged the half-life of DOX about 6 folds, which supported excellent stability of PDPP@D during blood circulation (Figure 4E and Table S5, Supporting Information). Real-time extravasation and tumor penetration of PDPP@D in 4T1 tumors were monitored (Figure 4F). After intravenous injection of PDPP@D, the signal was initially confined in the tumor blood vessels within the initial 30 min, and the nanoparticles then gradually extravasated from the vessels and diffused into the distal tumor site at 60 min. The biodistribution of PDPP and PDPP@D in mice bearing 4T1 tumors was investigated through the fluorescence detection (Figure 4G-H, Figure S37, Supporting Information). At 6 h after intravenous injection of PDPP and PDPP@D, Ppa fluorescence signal became distinctly visible at tumor sites in both PDPP and PDPP@D groups. As the time prolonged, stronger fluorescence signal in both PDPP and PDPP@D groups was observed in the solid tumor. The fluorescence signal in the PDPP@D-treated group was stronger than that in the PDPP group for all monitoring time points, because dual-responsive PDPP@D would exert the enhanced neighboring effect to initiate tumor penetration and retention. It was noted that Ppa retention was distinctly boosted in the PDPP@D-treated group at 18 d, and such an outstanding performance in tumor retention of Ppa was ascribed to deep penetration and homogeneous distribution of PDPP@D in the solid tumor tissue. Because of quick blood clearance and non-specific biodistribution of free Ppa, the Ppa-treated groups showed a very faint fluorescence signal throughout the monitoring process. The distribution of PDPP@D in 4T1 tumors at 24 h was imaged via observation of optical tumor sections under a CLSM (Figure 4I). These images confirmed the neighboring effect facilitated enhancement in PDPP@D extravasation from tumor vasculature into the distal matrix, thereby it may hold great potential for deep penetration in solid tumors.

This article is protected by copyright. All rights reserved.

Accepted Article

2.4. Antitumor effects of PDPP@D

The efficacy for treating malignant tumors with PDPP@D through a combined treatment strategy by PDT and chemotherapy was evaluated. The intracellular production of reactive oxygen species (ROS) of PDPP@D was shown in **Figure 5A**. 4T1 tumor cells treated with Ppa, PDPP and PDPP@D displayed similar enhanced green fluorescence as the positive control group (H_2O_2) after laser irradiation, and cells treated with PBS showed no detectable fluorescence signal. This result was consistent with photophysical properties of PDPP and PDPP@D in Table S2 (Supporting Information), which supported great performance of PDPP and PDPP@D for PDT.

PDPP and PDPP@D were less toxic against L02 normal cells in a dark condition compared with free Ppa (Figure 5B), indicating that PDPP and PDPP@D could decrease the cytotoxicity of Ppa by wrapping Ppa inside the nanoparticles. These results substantiated previous observations that nanocarriers from PEGylated dendritic peptides could effectively decrease the cytotoxicity of chemotherapeutic agents and photosensitizers against cancer because of their high biocompatibility.[10, 17] The effect of DOX encapsulation on the antitumor activity of PDPP@D was then investigated. Notably, the lowest viability was achieved at a molar ratio of 2:1 for Ppa to DOX in PDPP@D. The synergy of PDPP@D was quantified by calculating the combination index (CI) at different fraction affected (fa) values for each drug at the ratio of 2:1 (Figure 5C-D and Table S6, Supporting Information). PDPP@D at the Ppa/DOX ratio of 2:1 displayed the lowest CI values at a fa of 0.4 to 0.9 (IC40 to IC90), indicating an excellent synergism at the affected concentration. However, the physical mixture of Ppa and DOX only showed a synergism at a fa of 0.1 to 0.4 (IC10 to IC40) and the physical mixture of PDPP and DOX only exhibited a moderate synergism at a fa of 0.8 to 0.9 (IC80 to IC90). These results indicated that PDPP@D may have a stronger synergistic effect than the physical mixture from Ppa and DOX or PDPP and DOX on inhibiting tumor cells.

To investigate the *in vivo* antitumor effect of PDPP@D, the subcutaneous 4T1 tumor-bearing mice were employed as the animal model after intravenous administration of the product. As displayed in Figure 5E-H, the antitumor efficacy increased in the below order: saline < Ppa < DOX < Ppa+DOX < PDPP < PDPP@D. Although the group treated with the mixture of Ppa+DOX displayed reduced tumor burden compared to the groups treated with saline and single drugs, the overall efficacy of the

This article is protected by copyright. All rights reserved.

Accepted Article

mixture was significantly lower compared to that of PDPP and PDPP@D. In the meantime, PDPP@D showed a significantly higher tumor inhibition activity than PDPP. More importantly, after three successive injections of PDPP@D, the tumors gradually shrank and finally the tumors in three mice completely disappeared. Measurements of the tumor weight 17 days after the final treatment revealed that PDPP@D had a 98% tumor inhibition, significantly higher than PDPP (90%), supporting that dual-responsive PDPP@D with the neighboring effect was very efficacious in the combination therapy of tumors. Meanwhile, immunohistochemical studies confirmed that many terminal deoxynucleotidyl transferase-mediated dUTP nick end-labeling (TUNEL)-positive apoptotic cells were evidently observed in the tumor slides of mice treated with PDPP@D, whereas fewer positive cells in other groups Figure 5I. CD31 staining images suggested PDPP@D treatment had the best prognosis due to significantly decreased sign of tumoral angiogenesis (Figure S38, Supporting Information). The body weights of the mice treated with DOX and Ppa+DOX decreased noticeably, while no detectable abnormality of body weight was observed among the mice treated by PDPP@D (Figure S39, Supporting Information). H&E images also indicated a promising prognosis of PDPP@D treatment with no obvious sign of toxicity and metastasis (Figure S40, Supporting Information).

2.5. Irreversible ER stress induced by PDPP@D in tumor cells via transcriptome analysis

For deeper understanding of the mechanism of PDPP@D treatment to induce apoptosis of tumor cells, a transcriptome analytic approach was employed to detect alterations in gene expression or pathways in tumor cells after treatment with or without PDPP@D. Principal component analysis (PCA) revealed the majority of samples were clustered in the principal component 1 (PC1, x-axis), and all treatments including PD, PD+L (PD with laser irradiation), PDPP@D and PDPP@D+L (PDPP@D with laser irradiation) led to significant differences in gene expression compared to the control **(Figure 6A)**. Spearman rank correlation analysis indicated that gene expression in cells after these treatments had a strong negative correlation with those in the control.[18] Cells treated with PDPP@D+L were classified into a different cluster compared with those from other treatments (Figure 6B). The clusters of samples in PCA and correlation analysis collectively implied that treatment with PDPP@D+L could lead to significant changes in gene expression of 4T1 cells. In addition, treatment with both PD+L and PDPP@D+L resulted in more differentially expressed genes (DEGs) than their corresponding non-illuminated groups according to the DEGs presented in the

This article is protected by copyright. All rights reserved.

Accepted Article

volcano plots (Figure 6C and Figure S41, Supporting Information), which suggested the PDT effect of PDPP@D could be strongly related to major alterations in the cellular transcriptome and combination of PDT and chemotherapy was essential for regulating tumor cells. The pathways/processes with these DEGs after treatments were identified. Ingenuity pathway analysis (IPA) results suggested a high enrichment level of DEGs in cell cycle and apoptosis pathways, protein synthesis processes and collative signaling after treatment with PDPP@D+L (Figure 6D).

The ER stress triggers a signaling network known as the unfolded protein response (UPR) to restore the ER homeostasis, which promotes cell survival and adaptability.[19] However, under irreversible ER stress conditions, the UPR accelerates apoptosis.[19-20] PDPP@D+L had a greater impact on the UPR and induced the death receptor and apoptosis signaling pathways. The heatmap of comparison from IPA also supplied the evidence that PDPP@D+L distinctly reduced the growth of tumors and promoted the apoptosis and cell death of tumor cells (Figure S42, Supporting Information). Based on these findings, we hypothesized that PDPP@D+L would cause irreversible ER stresses, thus impairing the UPR and inducing apoptosis and cell death. The DEGs were selected via other analytic approaches and databases. The functional enrichment analyses based on the Kyoto Encyclopedia of Genes and Genomes (KEGG) database revealed that these DEGs induced by PDPP@D+L treatment were significantly enriched in cancer pathways,[21] cell cycle and genetic information processes, particularly protein synthesis process on the ER (Figure 6E and Figure S43-50, Supporting Information). The interaction network of these enriched KEGG pathways indicated disturbance of the protein synthesis process on the ER, particularly proteoglycan synthesis in tumor cells, could be the most significant contribution factor for apoptosis (Figure 6F and Figure S51-53, Supporting Information). Because DEGs were obtained from a cutoff value, we also employed gene set enrichment analysis (GSEA) to determine all significant genetic variations in cells were included as a set of genes in the pathways.[22] The result of GSEA demonstrated that PDPP@D+L treatment resulted in positively regulated pathways in inducing apoptosis and significantly inhibited protein synthesis processes on the ER (Figure 6G and and Figure S54, Supporting Information).

Experiments were conducted to measure the protein expression in the UPR after treatment of PDPP@D with laser irradiation at the same time as above transcriptome analysis, as well as at extended time points after treatment. As shown in Figure 6H and Figure S55 (Supporting

This article is protected by copyright. All rights reserved.

Accepted Article

Information), PDPP@D could up-regulate the expression of PKR-like ER kinase (PERK), one of the ER transmembrane proteins that initiate the UPR.[23] PDPP@D+L treatment could strengthen the eIF2α phosphorylation and induced the transcription factor C/EBP homologous protein (CHOP, Figure 5I and Figure S56, Supporting Information) to raise the mRNA level of death receptor 5 (DR5) expressed by *TNFSF10* gene (Figure 6J and Figure S57, Supporting Information). The DR5-associated caspase activation was also boosted after PDPP@D+L treatment evidenced with a significantly higher level of cleaved caspase-8 (cl-cas8) and cleaved caspase-3 (cl-cas3) that drive apoptosis.[24] Cleaved poly(ADP-ribose) polymerase (PARP) as a marker of apoptosis was remarkably increased (Figure 6H). Additionally, the level of these apoptosis-related markers was closely correlated with time after laser irradiation, indicating the process of cell death induced by PDPP@D+L treatment was positively regulated and not reversible (Figure 6H). Notably, the expression level of another ER protein, inositol requiring 1 (IRE1) that would inhibit apoptosis,[25] was significantly decreased after PDPP@D+L treatment, while the expression of binding immunoglobulin protein (BIP), which is an important protein for cytoprotection, slightly increased.[26] The above findings could support that PDPP@D+L treatment could lead to irreversible ER stresses and inhibition of cell protection through blocking the IRE1-dependent survival pathway and unleashing DR5-mediated caspase activity to drive cell death (Figure 6K).

3. Conclusions

In conclusion, we presented a versatile strategy based on dual-responsive dendritic polymer-based NPs PDPP@D to promote drug penetration in tumors through facilitating intracellular-to-intercellular delivery cycle via the neighboring effect. PDPP could effectively encapsulate DOX to prepare stable PDPP@D NPs at the feed ratio of DOX/PDPP obtained from DPD simulations, and PDPP@D exhibited delayed drug release to amplify the neighboring effect. In addition, LC/MS analysis confirmed that the released DOX and Ppa could escape from dying cells to kill neighboring cells. PDPP@D showed an enhanced efficacy by the combination of chemotherapy and PDT, which provided an encouraging approach to treat malignant tumors. Transcriptome studies demonstrated PDPP@D could activate the stress on the ER and block IRE1-associated cell protection, which resulted in irreversible stress with the evidence of a significantly raised DR5 level to increase the caspase activity and drive apoptosis. Distinctly, this study demonstrates an effective strategy to

This article is protected by copyright. All rights reserved.

Accepted Article

ameliorate drug penetration in solid tumors by amplifying the neighboring effect to overcome the tumor ECM barrier.

4. Experimental Section

Detailed experiments and methods, and other relevant data are available in the Supporting Information. All mouse experiments were in accordance with protocol approved by the Animal Ethics Committee of West China Hospital, Sichuan University (Approval No. 2019292A).

Supporting Information

Supporting Information is available from the Wiley Online Library or from the author.

Acknowledgements

Xiuli Zheng and Dayi Pan contributed equally to this work. This work was financially supported by National Natural Science Foundation of China (52073193, 82102197, 81801820, 51873120, 81621003), 1□3□5 project for disciplines of excellence, West China Hospital, Sichuan University (ZYJC21013), China National Postdoctoral Program for Innovation Talents (BX20200229), and the Fundamental Research Funds for the Central Universities. Apanpreet Bhamra was supported by the Engineering and Physical Sciences Research Council Doctoral Training Partnership (EPSRC DTP) Studentship. The authors would like to thank Li Li, Fei Chen and Chunjuan Bao from Laboratory of Pathology, West China Hospital, Sichuan University for helping with processing the historical sections and staining. Thanks to Qiqi Zhou from Institute of Clinical Pathology, West China Hospital of Sichuan University for for assistance with scanning the tissue slides. Thanks to Yaping Wu, Zhiqian Li, Lei Wu and Zhen Yang for assistance with CLSM image acquisition, and they are all from Core Facility of West China Hospital. Thanks to Xiaoting Chen from the Animal Experimental Center of West China Hospital for technical assistance in animal experiments. Thanks to Guiping Yuan from the Analytical and Testing Center of Sichuan University for morphology characterization work for her help of TEM images.

Conflict of Interest

The authors declare no competing interests.

This article is protected by copyright. All rights reserved.

Received: ((will be filled in by the editorial staff))
Revised: ((will be filled in by the editorial staff))
Published online: ((will be filled in by the editorial staff))

Accepted Article

References

[1] a) J. Ding, J. Chen, L. Gao, Z. Jiang, Y. Zhang, M. Li, Q. Xiao, S. S. Lee, X. Chen, *Nano Today* **2019**, *29*, 100800; b) J. Xiang, X. Liu, G. Yuan, R. Zhang, Q. Zhou, T. Xie, Y. Shen, *Adv. Drug Delivery Rev.* **2021**, *179*, 114027; c) N. Gong, Y. Zhang, X. Teng, Y. Wang, S. Huo, G. Qing, Q. Ni, X. Li, J. Wang, X. Ye, T. Zhang, S. Chen, Y. Wang, J. Yu, P. C. Wang, Y. Gan, J. Zhang, M. J. Mitchell, J. Li, X.-J. Liang, *Nat. Nanotechnol.* **2020**, *15*, 1053; d) Q.-S. Tong, W.-M. Miao, H. Huang, J.-Q. Luo, R. Liu, Y.-C. Huang, D.-K. Zhao, S. Shen, J.-Z. Du, J. Wang, *Small* **2021**, *17*, 2101208.

[2] a) F. Xu, X. Huang, Y. Wang, S. Zhou, *Adv. Mater.* **2020**, *32*, 1906745; b) J. Peng, Q. Yang, K. Shi, Y. Xiao, X. Wei, Z. Qian, *Adv. Drug Delivery Rev.* **2019**, *143*, 37; c) M. J. Mitchell, M. M. Billingsley, R. M. Haley, M. E. Wechsler, N. A. Peppas, R. Langer, *Nat. Rev. Drug Discovery* **2021**, *20*, 101.

[3] a) D. Huo, X. Jiang, Y. Hu, *Adv. Mater.* **2020**, *32*, 1904337; b) S. Thakkar, D. Sharma, K. Kalia, R. K. Tekade, *Acta Biomater.* **2020**, *101*, 43; c) H. Mohammadi, E. Sahai, *Nat. Cell Biol.* **2018**, *20*, 766; d) H. T. Nia, L. L. Munn, R. K. Jain, *Science* **2020**, *370*, eaaz0868.

[4] a) Y. Chen, X. Liu, H. Yuan, Z. Yang, C. A. von Roemeling, Y. Qie, H. Zhao, Y. Wang, W. Jiang, B. Y. S. Kim, *Adv. Sci.* **2019**, *6*, 1802070; b) W. Poon, B. R. Kingston, B. Ouyang, W. Ngo, W. C. W. Chan, *Nat. Nanotechnol.* **2020**, *15*, 819.

[5] a) X. Zhao, X. Yang, X. Wang, X. Zhao, Y. Zhang, S. Liu, G. J. Anderson, S.-j. Kim, Y. Li, G. Nie, *ACS Nano* **2021**, *15*, 14149; b) A. Zinger, L. Koren, O. Adir, M. Poley, M. Alyan, Z. Yaari, N. Noor, N. Krinsky, A. Simon, H. Gibori, M. Krayem, Y. Mumblat, S. Kasten, S. Ofir, E. Fridman, N. Milman, M. M. Lübtow, L. Liba, J. Shklover, J. Shainsky-Roitman, Y. Binenbaum, D. Hershkovitz, Z. Gil, T. Dvir, R. Luxenhofer, R. Satchi-Fainaro, A. Schroeder, *ACS Nano* **2019**, *13*, 11008; c) S. Chen, Y. Zhong, W. Fan, J. Xiang, G. Wang, Q. Zhou, J. Wang, Y. Geng, R. Sun, Z. Zhang, Y. Piao, J. Wang, J. Zhuo, H. Cong, H. Jiang, J. Ling, Z. Li, D. Yang, X. Yao, X. Xu, Z. Zhou, J. Tang, Y. Shen, *Nat. Biomed. Eng.* **2021**, *5*, 1019; d) K. Yang, Z. Yang, G. Yu, Z. Nie, R. Wang, X. Chen, *Adv. Mater.* **2022**, *34*, 2107434.

[6] D. Zhao, W. Tao, S. Li, Y. Chen, Y. Sun, Z. He, B. Sun, J. Sun, *Sci. Adv.* **2021**, *7*, eabg0880.

[7] a) I. de Lázaro, D. J. Mooney, *Nat. Mater.* **2020**, *19*, 486; b) J. Fang, W. Islam, H. Maeda, *Adv. Drug Delivery Rev.* **2020**, *157*, 142.

[8] C. Wang, S. Chen, Y. Wang, X. Liu, F. Hu, J. Sun, H. Yuan, *Adv. Mater.* **2018**, *30*, 1706407.

This article is protected by copyright. All rights reserved.

Accepted Article

[9] a) L. Adler-Abramovich, E. Gazit, *Chem. Soc. Rev.* **2014**, *43*, 6881; b) H.-W. An, L.-L. Li, Y. Wang, Z. Wang, D. Hou, Y.-X. Lin, S.-L. Qiao, M.-D. Wang, C. Yang, Y. Cong, Y. Ma, X.-X. Zhao, Q. Cai, W.-T. Chen, C.-Q. Lu, W. Xu, H. Wang, Y. Zhao, *Nat. Commun.* **2019**, *10*, 4861.

[10] X. Zheng, D. Pan, X. Chen, L. Wu, M. Chen, W. Wang, H. Zhang, Q. Gong, Z. Gu, K. Luo, *Adv. Sci.* **2021**, *8*, 2102741.

[11] a) F. Gong, N. Yang, X. Wang, Q. Zhao, Q. Chen, Z. Liu, L. Cheng, *Nano Today* **2020**, *32*, 100851; b) M. Grzelczak, L. M. Liz-Marzán, R. Klajn, *Chem. Soc. Rev.* **2019**, *48*, 1342; c) Y. Hou, W. Bu, H. Ai, Z.-R. Lu, T. Lammers, *Adv. Healthcare Mater.* **2021**, *10*, 2100243; d) L. Sun, F. Shen, L. Tian, H. Tao, Z. Xiong, J. Xu, Z. Liu, *Adv. Mater.* **2021**, *33*, 2007910; e) L. Luo, Y. Qi, H. Zhong, S. Jiang, H. Zhang, H. Cai, Y. Wu, Z. Gu, Q. Gong, K. Luo, *Acta Pharm. Sin. B* **2022**, *12*, 424; f) Q. Luo, Z. Duan, X. Li, L. Gu, L. Ren, H. Zhu, X. Tian, R. Chen, H. Zhang, Q. Gong, Z. Gu, K. Luo, *Adv. Funct. Mater.*, 2110408.

[12] a) C. Zhang, K. Pu, *Small Struct.* **2020**, *1*, 2000026; b) C. Zhang, Z. Zeng, D. Cui, S. He, Y. Jiang, J. Li, J. Huang, K. Pu, *Nat. Commun.* **2021**, *12*, 2934; c) S. He, J. Li, P. Cheng, Z. Zeng, C. Zhang, H. Duan, K. Pu, *Angew. Chem., Int. Ed.* **2021**, *60*, 19355; d) C. Xu, Y. Jiang, J. Huang, J. Huang, K. Pu, *Adv. Mater.* **2021**, *33*, 2101410.

[13] a) Y. H. Feng, X. P. Zhang, Z. Q. Zhao, X. D. Guo, *Mol. Pharmaceutics* **2020**, *17*, 1778; b) S. Zeng, X. Quan, H. Zhu, D. Sun, Z. Miao, L. Zhang, J. Zhou, *Langmuir* **2021**, *37*, 1225.

[14] X. Zheng, D. Pan, M. Chen, X. Dai, H. Cai, H. Zhang, Q. Gong, Z. Gu, K. Luo, *Adv. Mater.* **2019**, *31*, 1901586.

[15] J. L. Beesley, H. E. Baum, L. R. Hodgson, P. Verkade, G. S. Banting, D. N. Woolfson, *Nano Lett.* **2019**, *19*, 3386.

[16] M. E. Dolega, M. Delarue, F. Ingremeau, J. Prost, A. Delon, G. Cappello, *Nat. Commun.* **2017**, *8*, 14056.

[17] D. Zhong, H. Wu, Y. Wu, Y. Li, J. Yang, Q. Gong, K. Luo, Z. Gu, *J. Controlled Release* **2021**, *329*, 1210.

[18] P. Schober, C. Boer, L. A. Schwarte, *Anesth. Analg.* **2018**, *126*, 1763.

[19] T.-K. Chang, D. A. Lawrence, M. Lu, J. Tan, J. M. Harnoss, S. A. Marsters, P. Liu, W. Sandoval, S. E. Martin, A. Ashkenazi, *Mol. Cell* **2018**, *71*, 629.

[20] a) M. Lu, D. A. Lawrence, S. Marsters, D. Acosta-Alvear, P. Kimmig, A. S. Mendez, A. W. Paton, J. C. Paton, P. Walter, A. Ashkenazi, *Science* **2014**, *345*, 98; b) F. Xu, X. Li, X. Huang, J. Pan, Y. Wang, S. Zhou, *Sci. Adv.* **2020**, *6*, eabb8725.

This article is protected by copyright. All rights reserved.

Accepted Article

[21] M. Kanehisa, Y. Sato, *Protein Sci.* **2020**, *29*, 28.

[22] a) A. Subramanian, P. Tamayo, V. K. Mootha, S. Mukherjee, B. L. Ebert, M. A. Gillette, A. Paulovich, S. L. Pomeroy, T. R. Golub, E. S. Lander, J. P. Mesirov, *Proc. Natl. Acad. Sci.* **2005**, *102*, 15545; b) V. K. Mootha, C. M. Lindgren, K.-F. Eriksson, A. Subramanian, S. Sihag, J. Lehar, P. Puigserver, E. Carlsson, M. Ridderstråle, E. Laurila, N. Houstis, M. J. Daly, N. Patterson, J. P. Mesirov, T. R. Golub, P. Tamayo, B. Spiegelman, E. S. Lander, J. N. Hirschhorn, D. Altshuler, L. C. Groop, *Nat. Genet.* **2003**, *34*, 267.

[23] M. C. Kopp, N. Larburu, V. Durairaj, C. J. Adams, M. M. Ali, *Nat. Struct. Mol. Biol.* **2019**, *26*, 1053.

[24] C. Muñoz-Pinedo, A. López-Rivas, *Cell Death Differ.* **2018**, *25*, 226.

[25] J. H. Lin, H. Li, D. Yasumura, H. R. Cohen, C. Zhang, B. Panning, K. M. Shokat, M. M. LaVail, P. Walter, *Science* **2007**, *318*, 944.

[26] J. J. Rodvold, K. T. Chiu, N. Hiramatsu, J. K. Nussbacher, V. Galimberti, N. R. Mahadevan, K. Willert, J. H. Lin, M. Zanetti, *Sci. Signaling* **2017**, *10*, eaah7177.

This article is protected by copyright. All rights reserved.

Accepted Article

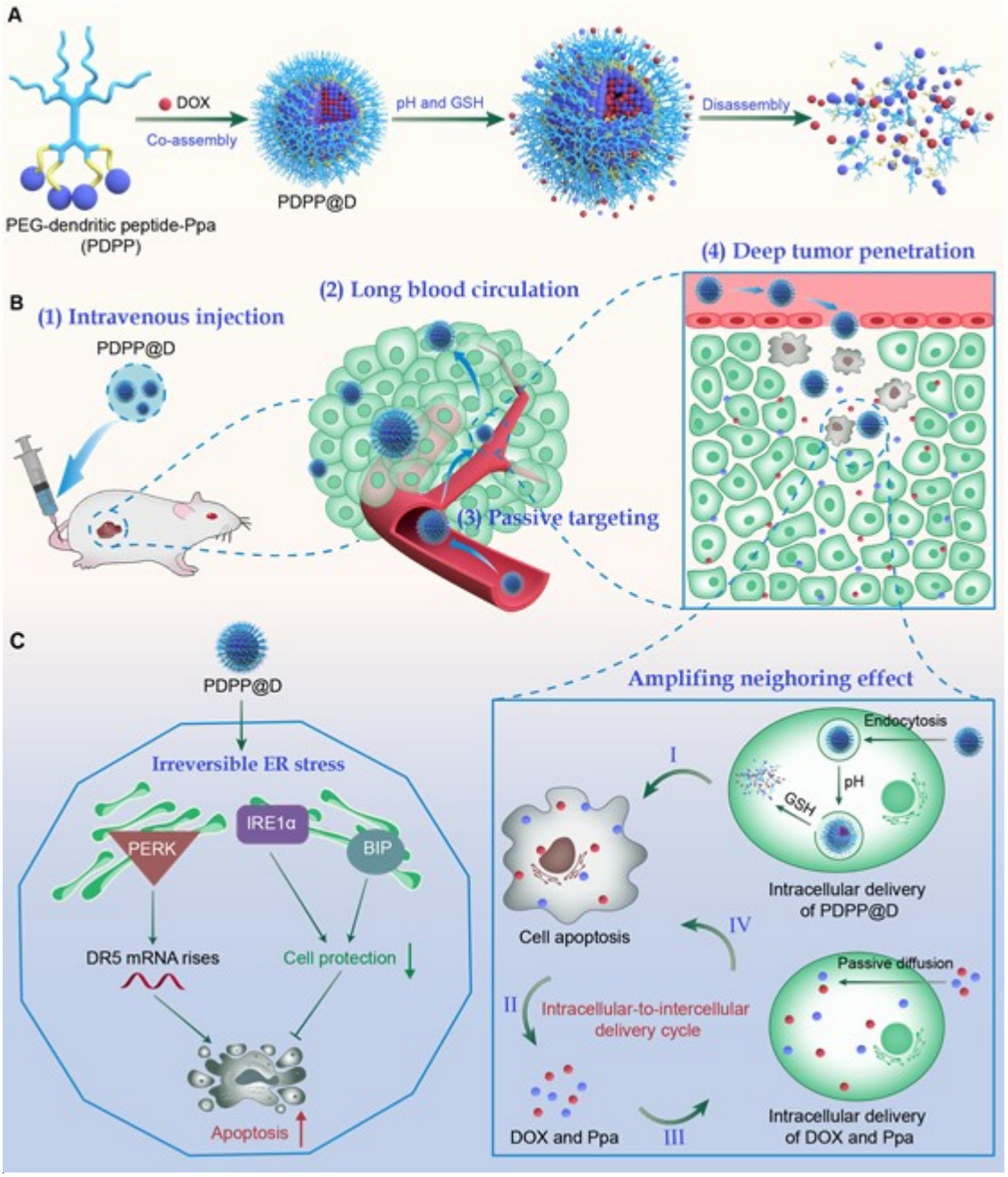

Figure 1. Schematic illustration for the formation of PDPP@D by self-assembly and its mechanism for enhancing the neighboring effect and inducing irreversible ER stresses. A) Self-assembly, drug loading and release process of PDPP@D. In response to an acidic pH and a high level of GSH in tumor cells, DOX and Ppa could be gradually released from PDPP, respectively. B) Deep penetration and anti-tumor destruction of DOX and Ppa mediated by PDPP@D through the neighboring effect in

This article is protected by copyright. All rights reserved.

Accepted Article

accompany with irreversible ER stresses. (1) After intravenous administration of PDPP@D, (2) Its circulation time in blood could be prolonged due to its ultrahigh stability, (3) prolonged blood circulation could facilitate efficient retention of PDPP@D in the tumor tissue via the EPR effect, and (4) enhanced retention and delayed drug release of PDPP@D could achieve its deep tumor penetration via the neighboring effect: (I) uptake of PDPP@D by tumor cells and release of DOX and Ppa in either an acidic pH or bio-reductive (GSH) environment; (II) Induction of cell apoptosis from released DOX and Ppa by a combination therapy of chemotherapy and photodynamic therapy; (III) Internalization of DOX and Ppa liberated from dying cells by neighboring cells; (IV) Induction of apoptosis of neighboring cells by released DOX and Ppa to create a intracellular-to-intercellular delivery cycle. This could ultimately enhance drug penetration and whole tumor destruction. C) Potential mechanism of PDPP@D. Intracellular accumulation of PDPP@D could induce irreversible ER stresses and inhibit cellular protection through blocking the IRE1-dependent survival pathways and enhancing the DR5-mediated caspase activity to drive cell death.

This article is protected by copyright. All rights reserved.

Accepted Article

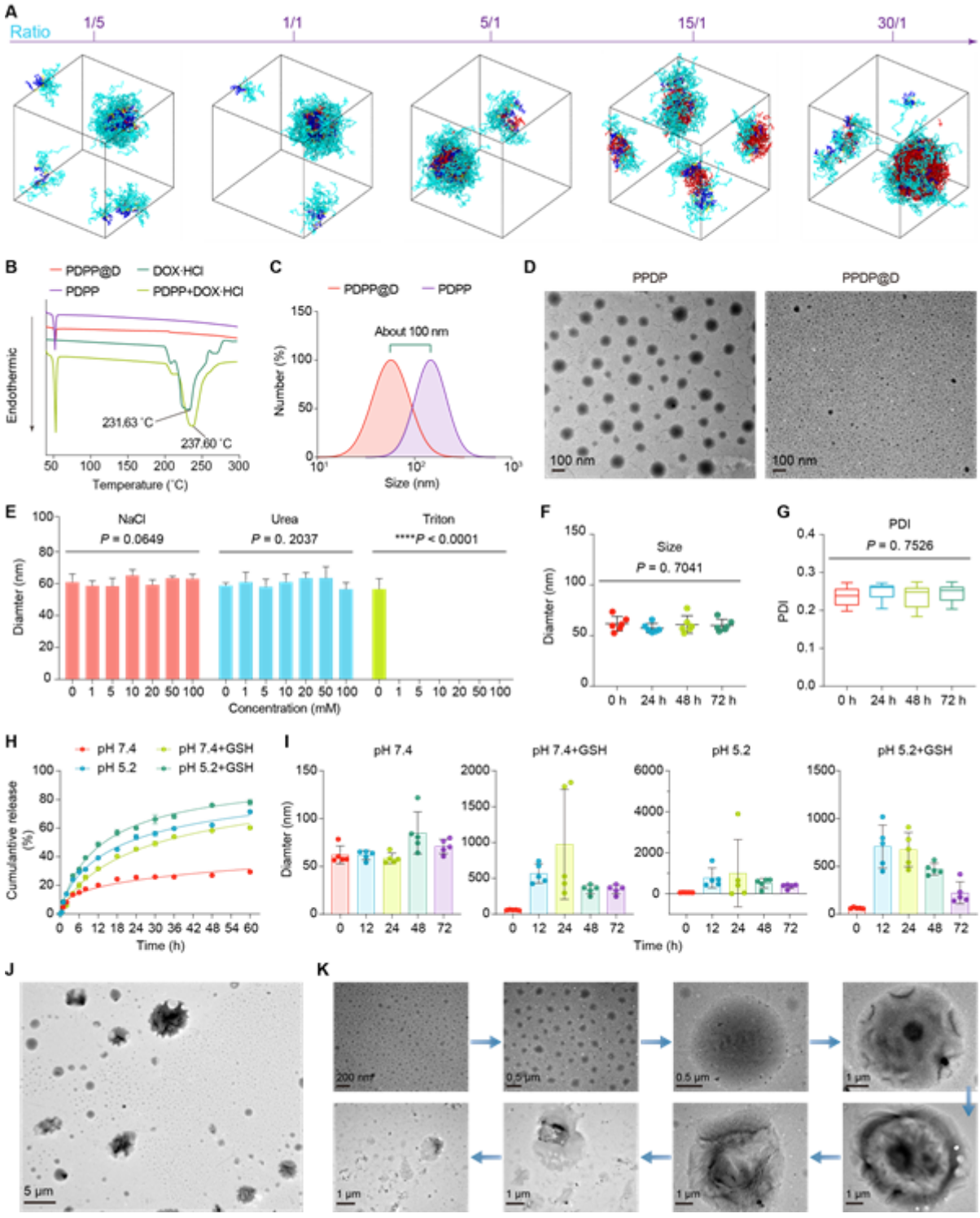

Figure 2. DPD simulations and physicochemical characterizations of PDPP@D. A) Side views of

This article is protected by copyright. All rights reserved.

Accepted Article

PDPP@D in H_2O at different ratios of DOX/PDPP from 1/5 to 30/1 at an equilibrium state. Coarse-grained Cambridge blue beads for PDP, dark blue beads for Ppa, red beads for DOX, and yellow beads for a disulfide bond. Water beads not shown for better clarity. B) Differential scanning calorimetry (DSC) curves of PDPP@D, PDPP, DOX·HCl, a physical mixture of PDPP and DOX·HCl. C) Hydrodynamic size distribution of PDPP and PDPP@D. D) Representative TEM images of PDPP and PDPP@D. E) Disassembly of PDPP@D after dissolving in NaCl, urea or Triton solutions (n = 5). F-G) Stability of PDPP@D in PBS with 10% FBS at 37 °C from 0 h to 72 h (F: variation in size; G: variation in PDI; n = 6). H) The cumulative DOX-release profile of PDPP@D under different release conditions. Three independent samples per group at each time point (n = 3). I) Size variations of PDPP@D under different release conditions at different incubation times (n = 5). J) TEM image of PDPP@D under the release condition (iv) for 24 h. K) TEM images for temporal structure evolution from self-assembly to disassembly of PDPP@D under the release condition (iv) for 24 h. After the initiation of size transition in acidic and reductive solutions, nanoparticles with multifarious sizes and morphologies, microparticles, irregularly micro-sized aggregates and degraded fragments were sequentially generated.

This article is protected by copyright. All rights reserved.

Accepted Article

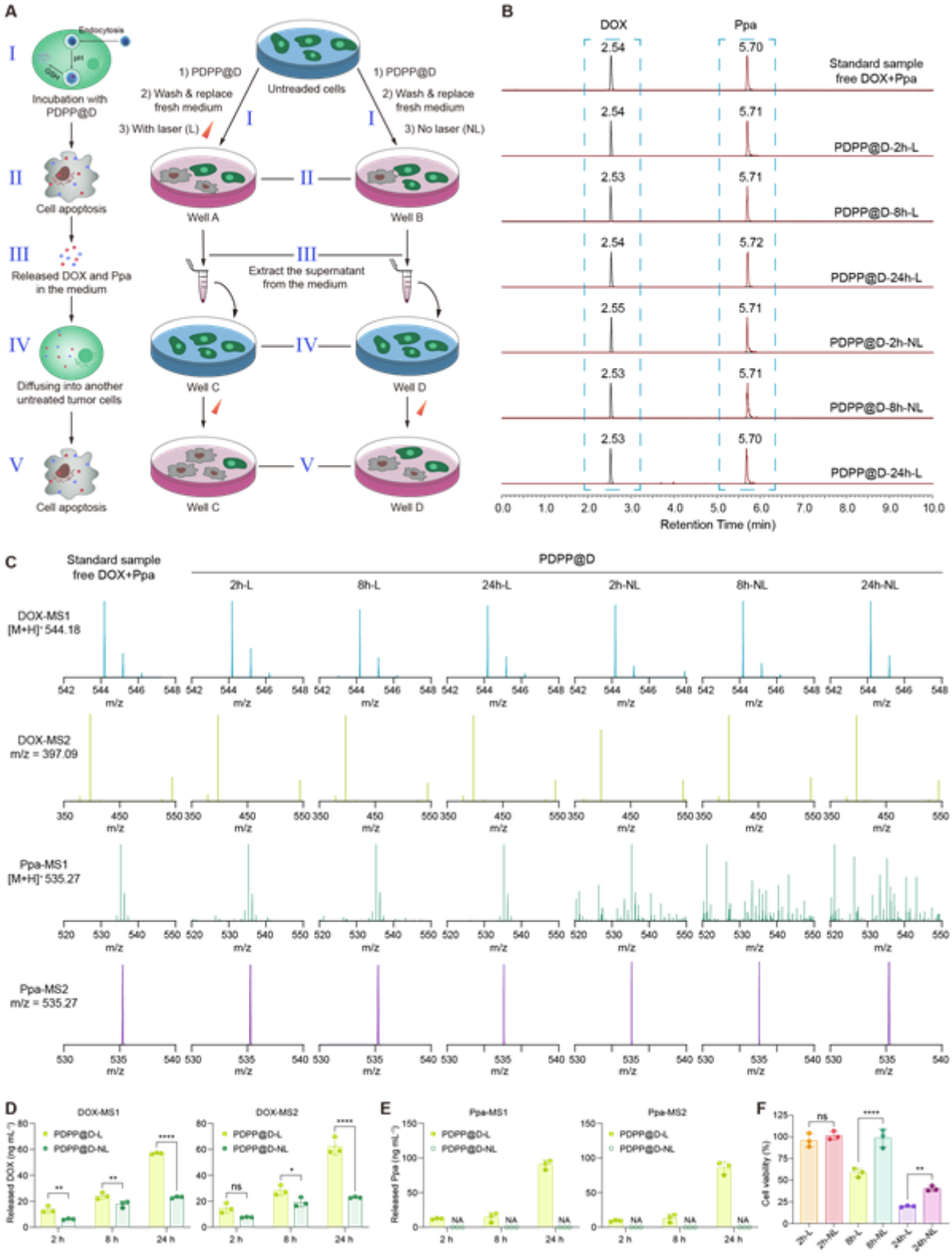

This article is protected by copyright. All rights reserved.

Accepted Article

Figure 3. The neighboring effect of PDPP@D. A) Schematic illustration of the experimental approach to confirm the neighboring effect of PDPP@D *in vitro*. The B) The LC/MS retention time of the released products in the spent medium collected from 4T1 cells incubated with PDPP@D for 2, 8, and 24 h with or without laser irradiation (well A and B in Figure 3A), in comparison with that of standard samples (free DOX and Ppa) under the same analytical condition. C). Analysis of the released products in the spent medium via mass spectrometry (MS, MS1) and tandem mass spectrometry (MS/MS, MS2) in comparison with standard samples (free DOX and Ppa) under the same analytical condition. D) Quantitative analyses of released DOX from 4T1 cells incubated with PDPP@D for 2, 8, and 24 h with or without laser irradiation (well A and B in Figure 3A) according to MS and MS2. E). Quantitative analyses of released Ppa from 4T1 cells incubated with PDPP@D for 2, 8, and 24 h with or without laser irradiation (well A and B in Figure 3A) according to MS and MS2. NA: not available. F) Cell viability of 4T1 cells (well C and D in Figure 3A) treated with the spent medium from 4T1 cells incubated with PDPP@D for 2, 8, and 24 h with or without laser irradiation (well A and B in Figure 3A). PDPP@D-L: PDPP@D treatment with laser irradiation; PDPP@D-NL: PDPP@D treatment without laser irradiation.

This article is protected by copyright. All rights reserved.

Accepted Article

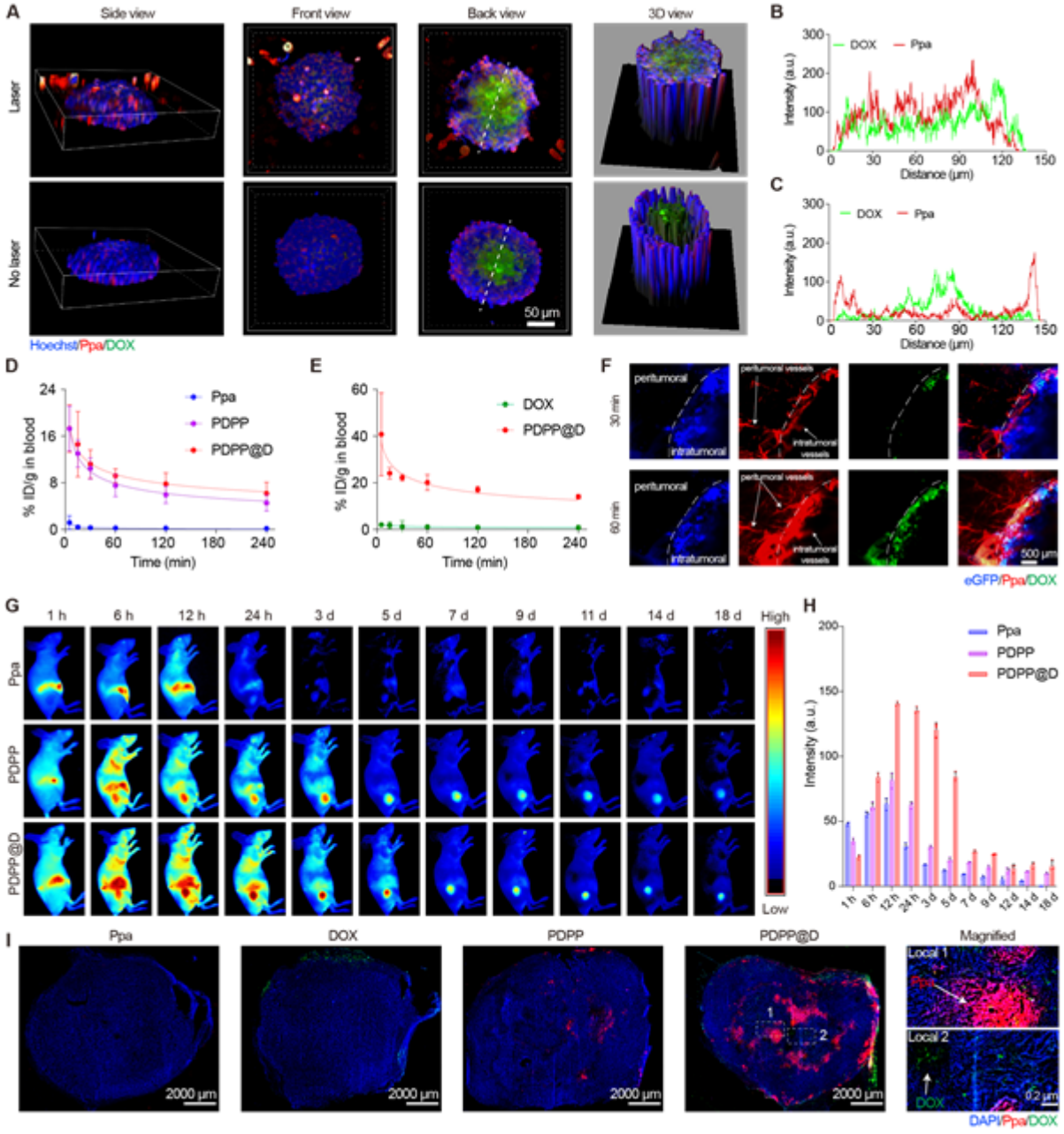

Figure 4. Enhanced penetration of PDPP@D via the neighboring effect *in vitro* and *in vivo*. A) 3D-reconstructed images for penetration of PDPP@D in 4T1 MTS with or without laser irradiation. Blue for cell nuclei; red for Ppa; and green for DOX. B) Line-scanning profiles of fluorescence intensity in the selected region of MTS after laser irradiation along the white line in (A). C) Line-scanning profiles of fluorescence intensity in the selected region of MTS without laser irradiation along the white line

This article is protected by copyright. All rights reserved.

Accepted Article

in (A). D) Blood clearance kinetics of PDPP, PDPP@D and Ppa (n = 5). E) Blood clearance kinetics of DOX and PDPP@D (n = 5). F) Confocal microscopy images of time-dependent penetration of PDPP@D from peritumoral vessels to the tumor tissues in mice at intervals after its injection. Blue for 4T1 cells; red for Ppa; and green for DOX. G) Fluorescence images of 4T1 xenografting tumor-bearing mice after intravenous injection of Ppa, PDPP and PDPP@D (n = 3). H) Quantitative fluorescence intensity of Ppa in tumors of mice in Figure 4G at different time points (n = 3). I) Fluorescence images of tumor cryosections for penetration of Ppa, DOX, PDPP and PDPP@D. Photo-irradiation was performed for Ppa, Ppa+DOX, PDPP and PDPP@D to induce the PDT effect. Blue for cell nuclei; red for Ppa; and green for DOX.

This article is protected by copyright. All rights reserved.

Accepted Article

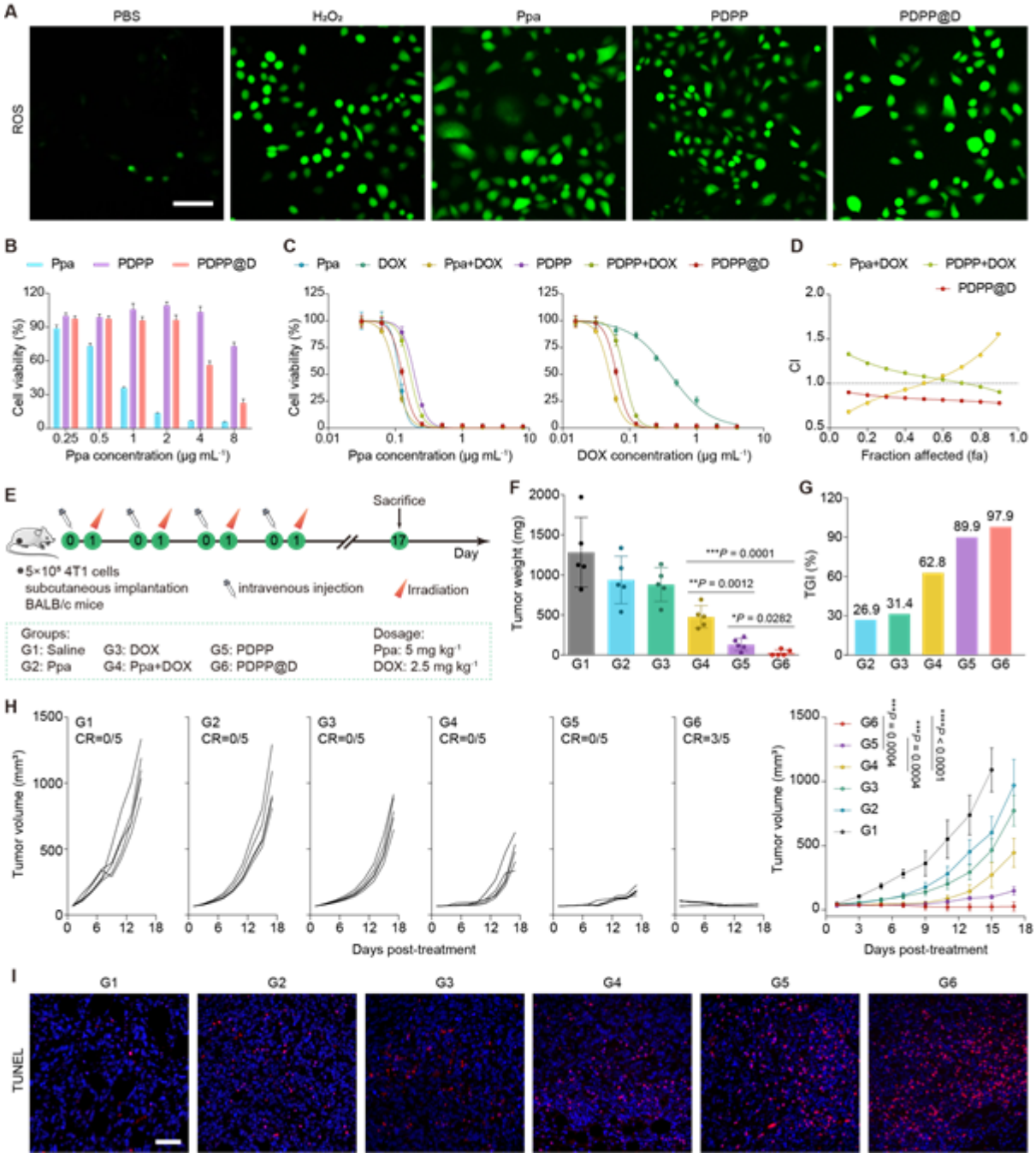

Figure 5. *In vitro* and *in vivo* anti-tumor efficacies of PDPP@D. A) ROS production by Ppa, PDPP and PDPP@D in 4T1 cells with PDT. Green for ROS-positive cells. Scale bar: 200 μm. B) *In vitro* cytotoxicity of Ppa, PDPP and PDPP@D against L02 cells in a dark condition determined by the CCK-8 assay (means ± SD, n = 3). C) Cytotoxicity of Ppa, DOX, Ppa +DOX, PDPP, PDPP+DOX and PDPP@D against

This article is protected by copyright. All rights reserved.

Accepted Article

4T1 cells. D) Combination Index (CI)-Fraction Affected (fa) curves of Ppa +DOX, PDPP, PDPP+DOX and PDPP@D against 4T1 cells. E) Schematic illustration of *in vivo* treatment (n = 5). G1: mice treated with saline as a control; G2: mice treated with free Ppa; G3: mice treated with free DOX; G4: mice treated with a mixture of free Ppa and DOX; G5: mice treated with PDPP; G6: mice treated with PDPP@D. F) Average tumor weight and (G) tumor growth inhibition (TGI) in each group in the 4T1 tumor model after *in vivo* treatment. H) Individual 4T1 tumor growth curves and average tumor growth curves in each group after *in vivo* treatment. I) TUNEL staining images of tumors at the experimental endpoint. Scale bars: 50 μm. To induce the PDT effect, photo-irradiation was performed for Ppa, Ppa+DOX, PDPP and PDPP@D unless otherwise specified.

This article is protected by copyright. All rights reserved.

Accepted Article

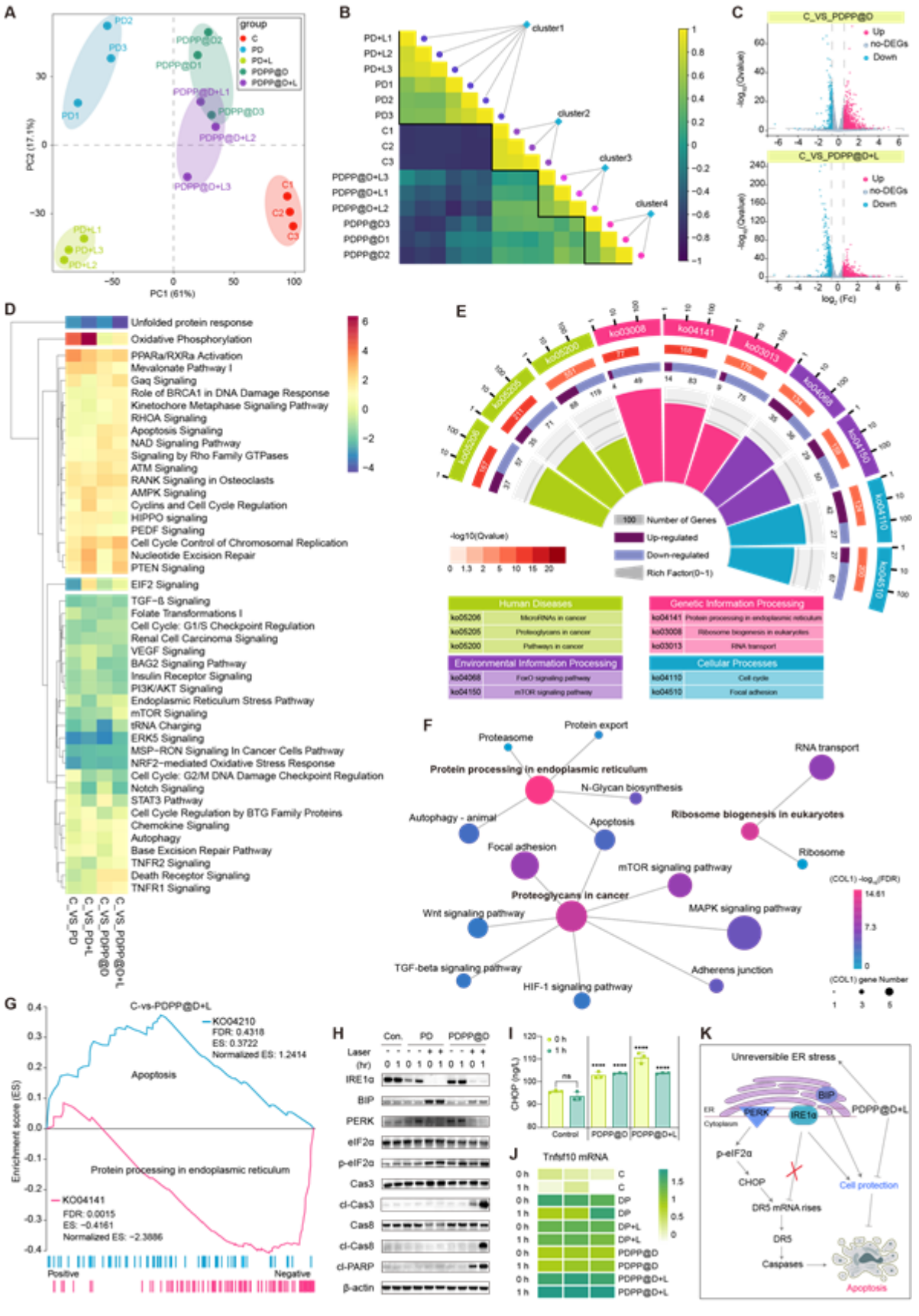

Accepted Article

Figure 6. Induction of irreversible ER stresses after treatment of PDPP@D to drive cell death. A) Principal components analysis (PCA) of normalized transcripts per million (TPM) in the transcriptome. C: untreated control; PD: Ppa+DOX treatment without laser irradiation; PD+L: Ppa+DOX treatment with laser irradiation; PDPP@D: PDPP@D treatment without laser irradiation; PDPP@D+L: PDPP@D treatment with laser irradiation. B) Heatmap of the Pearson correlation coefficient of the TPM of genes in each group. Samples in each group with the highest correlation coefficient (with a black line) suggested these parallel samples had great repeatability. C) Volcano plots for the DEGs in 4T1 cells after different treatments versus the control. Significance was indicated with a fold change in the absolute value > 1.5 and an *P* value of < 0.05 after ANOVA (n = 3). D) Heatmap of differentially regulated canonical pathways (*P* < 0.05) after different treatments by Ingenuity Pathway Analysis (IPA). Z-scores were calculated for the pathway enrichment and they were assigned with different colors. E) A circos image for highlighting top terms of the enriched pathways in the KEGG database from cells treated with PDPP@D+L. F) Interaction networks of the enriched KEGG pathways in cells treated by PDPP@D+L. G). GSEA of the pathways in cells treated by PDPP@D+L based on the KEGG database. H) Immunoblots of proteins in the UPR and apoptosis after treatment with PD and PDPP@D. I) Intracellular CHOP levels measured by ELISA after treatment with PDPP@D and PDPP@D+L compared with untreated cells as a control at the same time after laser irradiation. J). Relative expression level of *TNFSF10* genes after treatment with PD, PD+L, PDPP@D and PDPP@D+L through RT-PCR analyses. The expression data were log2 transformed for normalization. K) Schematic diagram of the effect of PDPP@D with laser irradiation on the UPR and cell death.

This article is protected by copyright. All rights reserved.

Accepted Article

The table of content

A versatile strategy based on dual-responsive nanosystem for combination therapy is developed to promote drug penetration in tumors through amplifying the neighboring effect, which may shed light on overcoming the tumor ECM barrier and eradicating solid tumors.

Xiuli Zheng, Dayi Pan, Guonian Zhu, Lu Zhang, Apanpreet Bhamra, Rongjun Chen, Hu Zhang, Qiyong Gong, Zhongwei Gu, Kui Luo*

A dendritic polymer-based nanosystem mediates drug penetration and irreversible endoplasmic reticulum stresses in tumor via neighboring effect

ToC figure

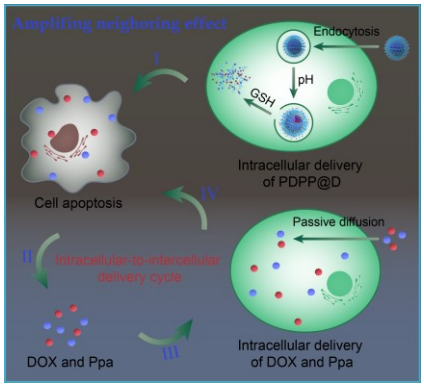

This article is protected by copyright. All rights reserved.